Exchange interactions and critical temperature of bulk and thin films of MnSi: A density functional theory study

Mahboubeh Hortamani,[1,2] Leonid Sandratskii,[2] Peter Kratzer,[1,3] Ingrid Mertig,[2,4] and Matthias Scheffler[1]
[1]*Fritz-Haber-Institut der Max-Planck-Gesellschaft, Faradayweg 4-6, D-14195 Berlin, Germany*
[2]*Max-Planck Institut für Mikrostrukturphysik, D-06120 Halle, Germany*
[3]*Fachbereich Physik, Universität Duisburg-Essen, D-47048 Duisburg, Germany*
[4]*Fachbereich Physik, Martin-Luther-Universität Halle-Wittenberg, D-06099 Halle, Germany*
(Received 4 June 2008; published 4 September 2008)

Recent theoretical work [H. Wu *et al.*, Phys. Rev. Lett. **92**, 237202 (2004); M. Hortamani *et al.*, Phys. Rev. B **74**, 205305 (2006); M. Hortamani, Ph.D. thesis, Freie Universität, Berlin, 2006] predicted ferromagnetism at zero temperature in thin MnSi films of B2-type crystal structure on Si(100). The relevance of this finding for finite-temperature experiments needs to be clarified by further investigations, since bulk MnSi is a weak ferromagnet with an experimentally measured Curie temperature of only T_c=30 K, and T_c is generally expected to be lower in thin films than in bulk materials. Here, we estimate T_c of such MnSi films using a multiple-sublattice Heisenberg model with first- and second-nearest-neighbor interactions determined from density functional theory calculations for various collinear spin configurations. The Curie temperature is calculated either in the mean-field approximation (MFA) or in the random-phase approximation (RPA). In the latter case we find a weak logarithmic dependence of T_c on the magnetic anisotropy parameter, which was calculated to be 0.4 meV for this system. In stark contrast to the above mentioned rule, large Curie temperatures of above 200 K for a monolayer (ML) MnSi film and above 300 K for a two ML MnSi film with B2-type structure on Si(100) are obtained within the RPA, and even higher values in MFA. Complementary calculations of MnSi bulk structures and thin unsupported MnSi films are performed in order to analyze these findings. We find that bulk MnSi in the cubic B2 structure is paramagnetic, in contrast to MnSi in the B20 ground-state structure in agreement with the Stoner criterion. In a tetragonally distorted B2 structure, the Mn atoms gradually develop a spin magnetic moment, passing through a low-spin and a high-spin state. However, the ferromagnetism of the MnSi/Si(100) films cannot be explained by tetragonal distortions alone, since the distorted B2 bulk structure is found to order antiferromagnetically. Comparison of the calculations of supported and unsupported films suggests that the reduced coordination of Mn atoms near surfaces and interfaces is crucial for the ferromagnetic ground state of the films. The coordination number of the Mn atoms in B2-type MnSi films on Si(100) constitutes a borderline case, where the spin magnetic moments of Mn are still large despite their sixfold coordination to Si, but the *sp-d* hybridization with Si states gives rise to a sizable ferromagnetic coupling of the Mn spins. We conclude that the Curie temperatures predicted from the Heisenberg Hamiltonian make thin MnSi films an interesting subject for further experimental investigation of spintronics materials.

DOI: 10.1103/PhysRevB.78.104402 PACS number(s): 75.50.Cc, 75.30.Et, 71.15.Mb

I. INTRODUCTION

One of the main goals of spintronics is to combine semiconductor technology with magnetic materials, aiming at the injection of a spin-polarized current from a ferromagnet into a semiconductor. The thin films of transition metals and their compounds on semiconductor substrates are considered as promising candidates for the fabrication of devices with desired functionality. In order to be employed for spin injection, the film should satisfy a number of conditions: (i) structural stability as an epitaxial film on the substrate; (ii) sharp and structurally well-defined interface with the substrate; and (iii) high temperature of the magnetic ordering and high degree of spin polarization at the Fermi level.

Earlier theoretical studies suggested the magnetic intermetallic compounds grown epitaxially on Si as promising candidates for spintronic applications.[1,2] The natural crystal structure of bulk MnSi is B20 type. Since, however, the B20 lattice has strong lattice mismatch with the Si(001) substrate, the epitaxially grown structure is expected to be of the tetragonally distorted cesium chloride (B2) type.[3–5] We found[2,3] that the MnSi B2 films have a high degree of spin polarization at the Fermi level between 30% and 50%, depending on film thickness; thus, this material is a candidate for spin injector.

The purpose of this paper is the study of the exchange interactions and the Curie temperature of the MnSi films on the Si(001) surface. As stated above a high Curie temperature is a necessary condition for the application of a magnetic system in spintronic devices.

This paper is organized as follows: In Sec. II we present the method of calculations and computational details. Section III is focused on structural, electronic, and magnetic properties of bulk MnSi. The bulk information forms a useful starting point for the analysis of the properties of the films. In Sec. IV we estimate the critical temperature of unsupported MnSi layers and thin-epitaxial MnSi films grown on Si. The results are summarized in Sec. V

II. THEORY AND COMPUTATIONAL DETAIL

Although density functional theory (DFT) is the best approach to describe the ground-state properties of systems, the

description of finite-temperature thermodynamic quantities, such as the Curie temperature, is not straightforward. A standard and convenient way to estimate the Curie temperature of an itinerant-electron system is to map the system on an effective Heisenberg Hamiltonian of interacting atomic magnetic moments.[6–9] For a multisublattice crystalline system, the Heisenberg Hamiltonian can be written in the form

$$H = -\sum_{i,j,\mu,\nu} J_{ij}^{\mu\nu} \mathbf{e}_{i\mu} \cdot \mathbf{e}_{j\nu}, \tag{1}$$

where the parameters $J_{ij}^{\mu\nu}$ describe the exchange interaction between two atoms; i and j are unit-cell indices; μ and ν are sublattice (basis site) indices; and $\mathbf{e}$ is the unit vector pointing in the direction of the magnetic moment at site (μ,i). Because of the crystal periodicity $J_{ij}^{\mu\nu}=J_{i-j,0}^{\mu\nu}$. The on-site exchange parameters in Eq. (1) are equal to zero: $J_{ii}^{\mu\mu}=0$. The vector $\mathbf{e}$ is assumed to take arbitrary directions that correspond to the classical treatment of atomic magnetic moment. This is a plausible description of itinerant-electron magnet.

The procedure of the mapping of an itinerant-electron system on the Heisenberg Hamiltonian consists of the determination of the interatomic exchange parameters $J_{ij}^{\mu\nu}$ on the basis of the first-principles calculations. In this paper we determine the exchange parameters by fitting the Heisenberg energies to the total energies of various collinear magnetic configurations. The details of the first-principles calculations are given below.

The Heisenberg Hamiltonian is used to estimate the Curie temperature. In the calculation of the Curie temperature, we employ two approaches: the mean-field approximation (MFA) and the random-phase approximation (RPA). For three-dimensional solids the MFA is expected to overestimate the value of the Curie temperature, whereas the RPA is expected to underestimate T_c.[10] The RPA gives better weighting of the spin-wave excitations than MFA and is supposed to give better estimation of the Curie temperature.

For the two-dimensional (2D) systems there is an additional complexity related to the Mermin-Wagner theorem. This theorem states that an isotropic 2D ferromagnet cannot order at nonzero temperature.[11] The reason for this is the gapless excitation spectrum of isotropic magnets. In the 2D systems the low-energy long-wavelength magnetic fluctuations destroy the long-range magnetic order at any nonzero temperature. If, however, the magnetic anisotropy is taken into account, the smallest excitation energy becomes nonzero. The value of the gap depends on the strength of the magnetic anisotropy. The gap in the excitation spectrum violates the conditions of the Mermin-Wagner theorem and leads to a nonzero value of the Curie temperature. The dependence of the Curie temperature on the anisotropy parameter has a logarithmic character and is relatively weak outside the range of very small anisotropy values. Since the dependence of the Curie temperature on the exchange parameters is approximately linear, for characteristic values of the magnetic anisotropy of the 2D ferromagnets, the magnitude of the Curie temperature is mostly determined by the strength of the exchange interactions.

The main physical quantity in the MFA is the effective exchange field experienced by a given magnetic moment from the side of all other magnetic atoms. The statistical mechanics in the MFA is the statistical mechanics of individual atomic spins in an effective exchange field originating from the interaction with the environment. The long-wavelength fluctuations are not present in the MFA and the conditions of the Mermin-Wagner theorem are violated; the MFA gives (for 2D isotropic ferromagnets) a nonzero value of the Curie temperature. On the other hand, the RPA deals with the wave-vector dependent spin-wave excitations and, in agreement with the Mermin-Wagner theorem, gives (for a 2D isotropic ferromagnet) a zero value of the Curie temperature. Thus, for the 2D systems the use of the RPA is strongly preferable. The MFA estimation of the Curie temperature can still be considered as a useful characteristic of the exchange interactions in the system. Therefore, in this paper we present both MFA and RPA estimations of the Curie temperature.

The MFA estimation of the Curie temperature of a multisublattice system can be obtained by solving the system of coupled equations,[12,13]

$$\langle e_\mu^z \rangle = \frac{2}{3k_B T_c} \sum_\nu J_0^{\mu\nu} \langle e_\nu^z \rangle, \tag{2}$$

where $J_0^{\mu\nu} \equiv \Sigma_j J_{0j}^{\mu\nu}$. Equation (2) can be rewritten in the form of an eigenvalue matrix problem,

$$(\Theta - T_c \mathrm{I})\mathrm{S} = 0, \tag{3}$$

where $\Theta_{\mu\nu}=(2/3k_B)J_0^{\mu\nu}$, $\mathbf{I}$ is a unit matrix, and $\mathbf{S}$ is the vector set of $\langle e_\nu^z \rangle$. The largest eigenvalue of the matrix gives the value of T_c^{MFA}.[12,13]

The RPA approach to the calculation of the Curie temperature of multiple-sublattice systems was recently discussed in Ref. 14. The derivation of the RPA method starts with the consideration of the Heisenberg Hamiltonian of quantum spins. Rusz *et al.*[14] arrived at the following formula:

$$k_B T_c = \frac{2}{3\langle \tilde{s}_\mu^z \rangle} \frac{S_\mu + 1}{S_\mu} \left\{ \frac{1}{\Omega} \int d\mathbf{q} [N^{-1}(\mathbf{q})_{\mu\mu}] \right\}^{-1}, \tag{4}$$

where $\tilde{s}_{i\mu}^z = S_{i\mu}^z / S_\mu$. Here $S_{i\mu}^z$ is the z component of the spin of the site (μ,i) and S_μ is the value of the spin of the atoms of the μ type. The average value of $\tilde{s}_{i\mu}^z$ does not depend on i. $[N^{-1}(\mathbf{q})_{\mu\mu}]$ in Eq. (4) is the diagonal element of the matrix inverse to matrix N defined by

$$N_{\mu\nu} = \delta_{\mu\nu} \left[\Delta + \sum_\eta J_{\mu\eta}(0) \langle s_\eta^z \rangle \right] - \langle s_\mu^z \rangle J_{\mu\nu}(\mathbf{q}). \tag{5}$$

Here k_B is the Boltzmann constant and Δ gives the magnetic anisotropy energy. The value of Δ can be estimated on the basis of first-principles calculations with the spin-orbit coupling taken into account. It is given by the energy difference of the ferromagnetic (FM) states with different directions of the magnetic moments. Equation (4) is written separately for each atomic type μ. Therefore, the number of equations is equal to the number of sublattices. These equations are interconnected through the matrix N [Eq. (5)]. Rusz *et al.*[14] suggested an iterational procedure for solving the system of Eq. (4). Since in this paper we consider the case of only two

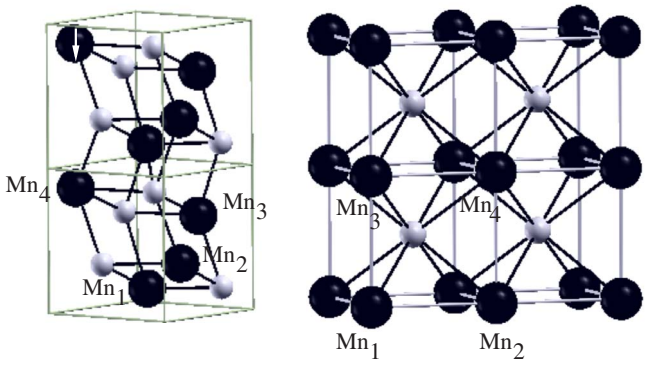

FIG. 1. (Color online) (a) Interlayer antiferromagnetic crystal structure of MnSi in B20 structure. The big black spheres are Mn and the small gray spheres are Si atoms. The B20 structure belongs to the $P2_13$ space group and has 4 Mn and 4 Si atoms in one simple-cubic cell at the positions (u,u,u), $(\frac{1}{2}+u,\frac{1}{2}-u,-u)$, $(-u,\frac{1}{2}+u,\frac{1}{2}-u)$, and $(\frac{1}{2}-u,-u,\frac{1}{2}+u)$ where $u_{\mathrm{Mn}}=0.137$ and $u_{\mathrm{Si}}=0.845$ (Ref. 17). (b) A $(2\times1\times2)$ unit cell of bulk MnSi in B2 (CsCl) crystal structure.

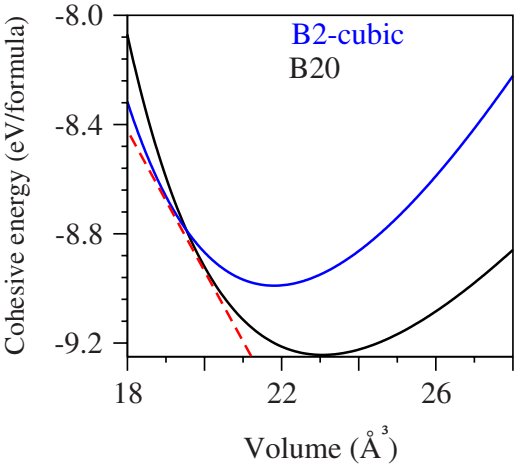

FIG. 2. (Color online) Energy-volume dependence of B20 (black curve), the B2-c structure (blue curve). The red dashed line is the common tangent of both curves. The pressure for the transition phase between the B20 and the B2-c structure is the slope of the red dashed line and is around 40 GPa.

inequivalent sublattices, the system of two equations is solved graphically.

As stated above for $\Delta=0$, the Curie temperature of a 2D system vanishes in agreement with the Mermin-Wagner theorem.[11]

The classical limit of Eq. (4) is obtained as a limit $S_\mu \to \infty$. Correspondingly, $(S_\mu+1)/S_\mu$ tends to be equal to one.

The DFT calculations were performed using the all-electron *full-potential augmented plane wave* plus *local-orbital* method[15] implemented in the WIEN code.[16] The exchange-correlation potentials are treated in the generalized gradient approximation (GGA-PBE96). The muffin-tin radii in the calculations for bulk MnSi are chosen to be $R_{\mathrm{MT}}=1.06$ Å for both Mn and Si. The convergency of the bulk calculations was achieved at the cutoff energy of $E_{\mathrm{cut}}^{\mathrm{wf}}=14.5$ Ry for the plane-wave expansion of the wave functions in the interstitial region. We used a $(15\times15\times15)$ **k** mesh in the first Brillouin zone.

The surface calculations are performed by means of a three-dimensional periodic supercell consisting of ten Si(001) layers followed by a maximum of five alternating atomic layers of Mn and Si and a vacuum spacer of about 10–11 Å (Fig. 1). The number of the substrate Si layers was chosen sufficiently large to reproduce the bulklike behavior of the central layers. The MnSi layers were assumed to have B2-type crystal structure. To make the system invariant with respect to space inversion, the MnSi films were put symmetrically at both the top and the bottom of the Si slab. The calculated equilibrium lattice constant of bulk Si (5.48 Å) is used for the Si(001) substrate. In the film calculations, the muffin-tin radii are chosen to be 1.06 Å for both Mn and Si as used in our previous calculations.[1–3,18,19] The energy cutoff convergency for the film was achieved using $E_{\mathrm{cut}}^{\mathrm{wf}}=13.8$ Ry for the plane-wave expansion in the interstitial region. A set of $(10\times10\times1)$ special **k** points is used for integrations over the Brillouin zone of the (1×1) surface cell of Si(001). In the film calculation, all Mn and Si layers except the two central Si layers in the slab are relaxed until the calculated atomic forces are smaller than 0.03 eV/Å.

III. BULK MnSi

The intermetallic compound MnSi is known to form a cubic crystal structure B20 with four Mn and four Si atoms per unit cell. Other transition-metal silicides such as FeSi, CoSi, and CrSi also crystallize in this type of structure. The point group is $P2_13$. It includes four threefold rotation axes pointing in the (111), $(1\bar{1}\bar{1})$, $(\bar{1}1\bar{1})$, and $(\bar{1}\bar{1}1)$ directions. The calculated lattice parameter in the present work is 0.9% smaller than the experimental value. The Mn atom has one Si neighbor at 2.28 Å along the [111] direction, three Si neighbors at a distance of 2.37 Å, and three Si neighbors at 2.52 Å [see Fig. 1(a)].

Below the magnetic critical temperature of 29 K, MnSi has a helical magnetic structure with a long spiral period of 180 Å. The formation of the helical structure in MnSi is a consequence of relativistic effect and the lack of inversion symmetry.[17,20]

The B20 crystal lattice cannot be matched with the Si(001) substrate. We consider the CsCl-type (B2) lattice [Fig. 1(b)] as an epitaxially grown structure of MnSi on Si(001). The B2 lattice matches well with the Si surface. The B2 films of FeSi and CoSi have been successfully grown by von Känel *et al.*[21] on Si(111). A recent work[1] predicted the B2 crystal structure for MnSi films on Si(001).

In this section we report the results of the calculations for bulk MnSi with both B20 and B2 structures. The comparison of the calculated properties of the bulk, the surface, and the film of MnSi allows one to get a deeper insight into the physics of the systems. For the B2 lattice, we will study the role of the tetragonal distortions (B2-t). We will refer to the undistorted B2 lattice as cubic B2 lattice (B2-c). In Fig. 2 we present the total energy versus volume plot for the B20 and the B2-c lattices. The curves were fitted using the Mur-

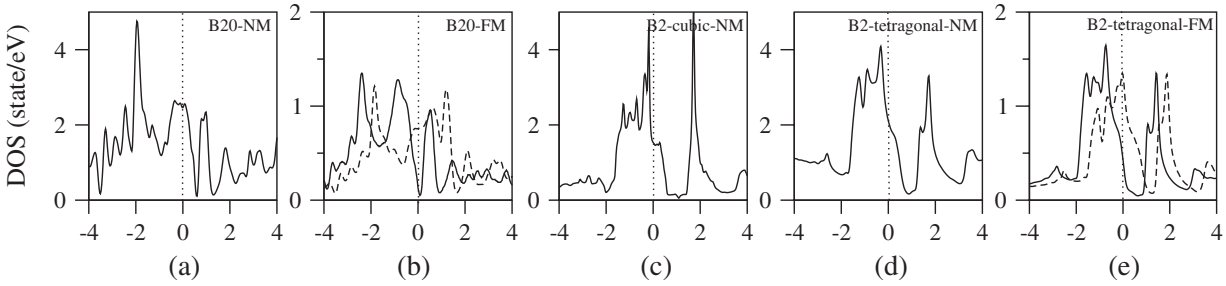

FIG. 3. Density of states for MnSi in the B20 structure using a mesh of $(18\times18\times18)$ k points in the Brillouin zone. (a) The solid line is the DOS of the B20 structure in the nonmagnetic phase for both spin channels. (b) The solid (dash) line is the DOS of the majority (minority) spin channel. (c) and (d) The solid line is the DOS of the nonmagnetic phase for cubic and tetragonal structures. (e) The solid (dash) line is the DOS for the B2 in the majority (minority) spin channel. The Fermi level is set to be the energy zero.

naghan equation. The equilibrium energy of the B2-c structure exceeds the equilibrium energy of the B20 structure by 0.25 eV/formula unit. This energy difference is less than the corresponding differences for FeSi (0.04 eV) and CoSi (0.42 eV).[4] The calculations show that equilibrium MnSi in B20 structure is ferromagnetic while in B2-c structure it is paramagnetic (PM). In the B20 phase, the antiferromagnetic (AFM) state is energetically higher by 52 meV/formula unit than the FM state. The atomic Mn moment in the AFM structure of the B20-MnSi is 0.48 μ_B. The induced moment on Si is in this case zero. In the FM state the corresponding atomic moments are 1.03 (0.04) μ_B, which are larger than the experimental moment of 0.4 μ_B per formula unit. The calculated atomic moments are comparable to the results of recent calculations by Jeong and Pickett[22] performed with the full-potential local-orbital method. We calculate the atomic spin moments for the muffin-tin spheres with a radius of 1.06 Å. This radius is 5% smaller than the radius of the touching spheres for the B20 lattice. The consideration of the touching atomic spheres does not change the atomic moments substantially.

The equilibrium lattice constant for the metastable B2-c structure is 2.79 Å (Fig. 2) that is close to half of the calculated lattice constant of Si 5.48 Å. Therefore, the mismatch between lattices is less than 2% and Si can be considered as a good substrate to grow B2 MnSi layers.

The B2 structure can be stabilized by high pressure. The GGA calculations show a phase transition from the B20 to the B2 structure at a pressure of about 40 GPa (Fig. 2). The value of the critical pressure is given by the slope of the common tangent to the energy-volume curves for both B2 and B20 structures: $p=-(\partial E/\partial V)_T$. This pressure is larger than the critical pressure that suppresses the magnetism in the B20 structure.[23]

At the corresponding equilibrium volumes, the B20 MnSi is ferromagnetic while the B2-c MnSi is nonmagnetic. The difference in the magnetic state of these two phases can be explained on the basis of the Stoner criterion,[24] which states that a nonmagnetic state of a system is unstable with respect to the formation of the ferromagnetic state if $IN_{\mathrm{nm}}(\epsilon_F)>1$, and it is stable if the value of the product is smaller than one. Here I is the Stoner parameter and $N_{\mathrm{nm}}(\epsilon_F)$ is the density of states (DOS) at the Fermi level in the nonmagnetic phase.

In Figs. 3(a) and 3(c) we show the DOS of the nonmagnetic states of both B20 and B2-c structures. The B20 DOS is broader than the B2-c DOS. This can be attributed to the shorter Mn-Si bond length in the B20 structure. However, the Fermi level of the B20 DOS lies on one of the local peaks while for the B2-c structure the Fermi level is at a shoulder of a peak with smaller value of the density of states.

The Stoner parameter can be estimated according to the formula: $I=\Delta_{ex}/m$, where Δ_{ex} is the exchange splitting between spin-up and spin-down states and m is the corresponding magnetic moment giving the origin to the exchange splitting. The value of Δ_{ex} is estimated from the DOS of the B20 structure as the energy distance between corresponding peaks in the spin-up and spin-down DOSs. The calculated $\Delta_{ex}=0.55$ eV and $m=1.0$ μ_B yield a Stoner parameter of $I=0.5$ eV/μ_B. This value is comparable with the Stoner parameter of fcc Mn, 0.41 eV/μ_B, reported by Janak.[25] The Stoner parameter can be treated as an atomic characteristic that does not depend substantially on the crystal environment.[26] Therefore, we use the same Stoner parameter for both B2 and B20 structures.

The values of the Stoner product are given in Table I. For the B20 structure the Stoner product exceeds unity and predicts the ferromagnetic instability, whereas for the B2-c structure, it is substantially smaller than unity and the ground state of the system is nonmagnetic.

TABLE I. Density of states per Mn atom at the Fermi level for both spin channels $N_\uparrow(\epsilon_F)$ and $N_\downarrow(\epsilon_F)$, total density of states at the Fermi level for the nonmagnetic case $N_{\mathrm{nm}}(\epsilon_F)$ (state/eV), the exchange splitting Δ_{ex} (eV), the product of Stoner parameter I, and $N_{\mathrm{nm}}(\epsilon_F)$.

	$N_{\mathrm{nm}}(\epsilon_F)$	Δ_{ex}	IN_{nm}	$N_\uparrow(\epsilon_F)$	$N_\downarrow(\epsilon_F)$
B20	2.5	0.55	1.25	0.5	0.6
B2-c	1.5		0.75		
B2-t	2.1	0.4	1.05	0.6	1.8

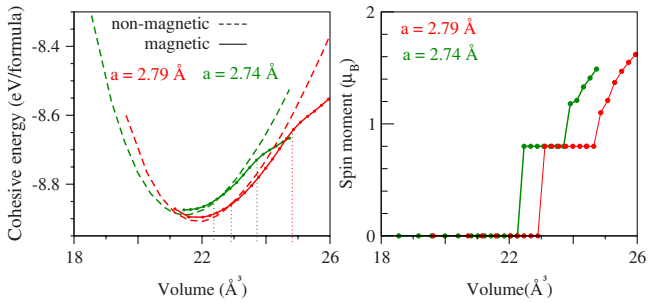

FIG. 4. (Color online) (a) B2 in tetragonal structure with in-plane lattice constant of 2.74 Å (green curve) and 2.79 Å (red curve). Dashed lines are for the nonmagnetic state and solid lines are for the FM state. (b) The magnetic moment per formula unit in the tetragonal B2 structure. The magnetic moment of PM, LS, and HS states are clearly resolved in this plot.

Note that for the B2-c structure, an antiferromagnetic state exists. The Mn moments assume a small value of 0.17 μ_B. The energy of the antiferromagnetic state is 6 meV per Mn atom higher than the energy of the nonmagnetic state.

Since the epitaxial growth of the MnSi films on Si(001) is accompanied by tetragonal distortions, we performed calculations for the bulk MnSi with a distorted B2 lattice. The calculations were performed as follows. The a and b parameters of the base plane of the structure were fixed either to $a=b=2.79$ Å (the equilibrium lattice constant of the B2-c MnSi) or to $a=b=2.74$ Å that corresponds to the lattice constant of Si. The c parameter of the tetragonally distorted structure was varied. The magnetic structure appears in the first case at $c=1.05\ a$, while using the Si lattice constant, the magnetic structure is stabilized at $c=1.10\ a$. In both cases the transition from the equilibrium nonmagnetic structure to the equilibrium ferromagnetic structure is discontinuous; the magnetic moment per atom jumps from 0 to 0.8 μ_B (Fig. 4). The tetragonal distortion leads to an increase in the DOS at the Fermi level of the nonmagnetic state (Fig. 3) that is the origin of the ferromagnetic instability in agreement with the Stoner picture.

The energies of the structures as a function of volume are presented in Fig. 4(a). The corresponding dependencies of the atomic spin moments are given in Fig. 4(b). The characteristic feature of the tetragonally distorted B2-t is the presence of two discontinuous phase transformations. As already mentioned, in the low-volume region the system is nonmagnetic. With increasing volume, the system first transforms into a low-spin (LS) ferromagnetic state. Further increase in the volume leads to the discontinuous transformation to a high-spin (HS) state. These transformations lead to discontinuities of the first derivative of the energy as a function of volume. In contrast to the tetragonally distorted systems, the volume variation for the B2-c does not lead to a discontinuous phase transformation. With an expansion of the system, it reaches a critical point of the appearance of ferromagnetism. With further increase in the volume, the magnetic moment increases, continuously staying, however significantly, lower than the high-spin moment of the distorted phases. These results show that the tetragonal distortions of the B2 phase inherent for the epitaxially grown films enhance the trend to the formation of a magnetic state.

Next we estimate the magnetic transition temperature for the B2 structure with the Si lattice parameters $a=b=2.74$ Å and $c=3.1$ Å. For these lattice parameters the ferromagnetic state has the LS type. Our calculation shows that the antiferromagnetic state, which has a checkerboard structure in the xz plane, has its energy lower than the ferromagnetic state by 16 meV/Mn. Therefore, we estimate the Néel temperature of this antiferromagnetic state. To estimate the exchange field experienced by the magnetic moments, we compare the energy of the ground antiferromagnetic state and the energy of the configuration in which one of the spins is reversed. This energy difference is 40 meV. Under a simplified assumption about the character of the interatomic exchange interactions, we get on the basis of the mean-field approximation the value of the Néel temperature of 60 K.

IV. THIN FILMS

The epitaxial thin films of some materials grow in a crystal structure that is different from their bulk structure (pseudomorphical growth). This property is explained by the presence of the strain and/or interface and surface energy contributions. The studies of the structural stability and magnetic properties of pseudomorphically grown MnSi in B2 structure on Si(001) are reported earlier.[1,2,5] The unit cell of the B2 structure is rotated by 45° with respect to the Si(001)(1×1) surface unit cell. The surface unit cell of a one monolayer (ML) B2 film contains two inequivalent Mn at-

TABLE II. Total energies and magnetic moments of various magnetic configurations of one ML MnSi. The surface supercell contains four Mn atoms numbered according to Fig. 5(a). The energy of the ferromagnetic state is taken as the energy zero. +/− present up/down directions of spins of Mn atoms.

Magnetic Configuration	$E_{MC}-E_{FM}$ eV/(2×1) cell	Mn_1 μ_B	Mn_2 μ_B	Mn_3 μ_B	Mn_4 μ_B
FM(++++)	0	2.16	2.16	1.61	1.61
MC1(+++−)	0.261	2.18	2.18	1.75	−2.37
MC2(+−++)	0.252	2.15	−1.73	2.21	2.21
MC3(++−−)	0.443	1.87	1.87	−2.53	−2.53
MC4(+−+−)	0.291	2.05	−2.05	2.22	−2.22

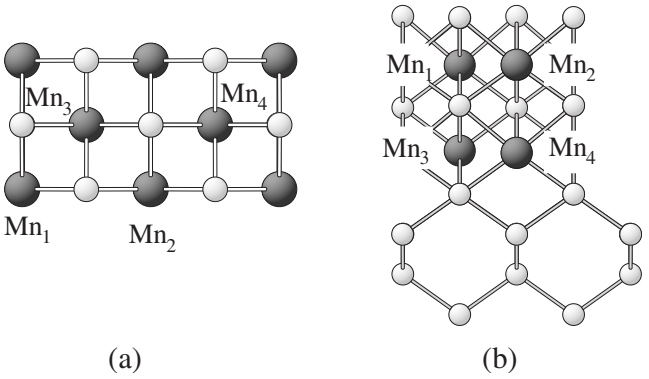

FIG. 5. (a) Top view of one ML (with a (2×1) in-plane surface unit cell) and (b) side view of two MLs [with a (1×1) in-plane surface unit cell] MnSi/Si(001). Black circles are Mn and gray circles indicate Si atoms.

oms that sit at the bridge sites of the Si(001)(1×1) surface. We have shown that the Mn moments in this film are ferromagnetically coupled. We found previously that the films are ferromagnetic up to two MLs. With further increase in the film thickness, an interlayer antiferrimagnetic order becomes favorable.[1,2] An important question is if the ferromagnetic order of the one and two ML films of MnSi is retained at room temperature. Answering this question requires the knowledge of the interatomic exchange interactions.

In this section we estimate the Curie temperature on the basis of first-principles calculations of the Mn-Mn exchange parameters. The exchange parameters are evaluated by fitting the DFT energies of a number of collinear magnetic configurations with a Heisenberg Hamiltonian. A larger number of magnetic configurations leads to a larger number of the exchange parameters that can be obtained by the fitting. The number of the considered collinear magnetic configurations is restricted by the size of the magnetic supercell used in the calculations. Since the calculation for large super cells with the WIEN package is very expensive, we evaluated parameters for near neighbors only. Previous calculation of exchange interaction for various systems show that, in compounds, the exchange parameters are expected to decay rapidly with an increasing distance between the magnetic atoms, and the restriction to nearest neighbors is reasonable.[27] In the following the Curie temperature is calculated for the films consisting of one or two MLs.

We begin with the consideration of one ML. The in-plane exchange couplings for the first- and second-nearest neighbors are obtained for the case of one ML of MnSi using a (2×1) surface unit cell containing four MnSi formula units [Fig. 5(a)].

The first-neighbor interaction is between Mn atoms in the corner (Mn_1) and in the middle (Mn_3) of Fig. 5(a). In the second Mn neighbor interactions, Mn atoms are both located either in the corner (Mn_1 and Mn_2) or in the middle (Mn_3 and Mn_4) [Fig. 5(a)]. For the selected supercell there are five inequivalent collinear magnetic configurations (MCs). MC1 and MC2 are antiferrimagnetic while MC3 and MC4 are antiferromagnetic. The energies and magnetic moments of these configurations are collected in Table II. The inspection of the energies of the magnetic configurations shows that the energy of MC3 is much higher than the other configurations. Since a characteristic feature of MC3 is an antiparallel orientation of the moments of all nearest neighbors, this high energy reveals a strong ferromagnetic interaction between nearest neighbors.

We found that the following exchange parameters reproduce well the energies of magnetic configurations collected in Table II. The parameter of the nearest-neighbor interaction is 13.8 meV. The second-nearest-neighbor interactions between the Mn_1 and the Mn_2 (the Mn_3 and the Mn_4) are 3.8 (4.9) meV. As expected, the exchange interaction with second neighbors is significantly smaller than with the nearest neighbors. The nearest-neighbor interaction determines substantially the value of the Curie temperature.

In the case of the two ML films, we use a (1×1) surface unit cell to evaluate the interlayer exchange parameters, i.e., two sublattices per layer. On the basis of this unit cell, we can calculate the first-neighbor in-plane exchange parameter for both surface and interface layers. Since the surface and interface Mn layers have different Si environments, the exchange interactions within layers can be different. The first-neighbor interlayer exchange interaction is between Mn_2-Mn_4 and Mn_1-Mn_3 [Fig. 5(b)]. The second-neighbor interlayer exchange interaction is between Mn_1-Mn_4 and Mn_2-Mn_3.

To estimate the exchange parameters, we consider five magnetic configurations. Their energy and magnetic moments are given in Table III. The comparison of the energies of magnetic configurations shows that MC1 and MC2 have very similar high energies, whereas the energies of the MC1 and MC4 are much smaller. The following set of parameters

TABLE III. Total energies and magnetic moments of various magnetic configurations of two ML SiMn. The surface supercell contains four Mn atoms in two layers, numbered according to Fig. 5(b). The energy of the ferromagnetic state is taken as energy zero.

Magnetic Configuration	$E_{MC}-E_{FM}$ eV/cell	Mn_1 μ_B	Mn_2 μ_B	Mn_3 μ_B	Mn_4 μ_B
FM(++++)	0	1.00	1.26	1.98	1.81
MC1(+++−)	0.356	1.44	0.74	1.87	−1.88
MC2(+−++)	0.151	0.60	−0.60	2.06	1.74
MC3(+−+−)	0.345	1.00	−1.24	2.01	−2.01
MC4(++−−)	0.065	0.65	1.54	−2.13	−1.75

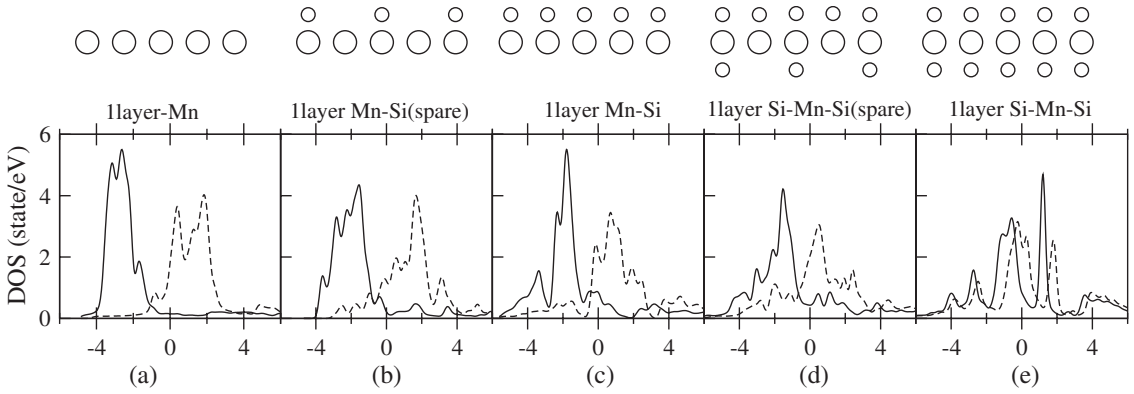

FIG. 6. Density of states of the Mn atom in the unsupported free-standing layer. (a) A single Mn layer, (b) Mn-Si (sparse) layer, (c) Mn-Si (dense) layer, (d) Mn layer sandwiched between two asymmetric Si dense and sparse layers, and (e) Mn layer sandwiched between two symmetric Si layers. The Fermi level is set to the energy zero. The schematic of each structure is shown above the plots, small circles are Si and large circles are Mn atoms.

describe these energies: The in-plane parameter for the Mn atoms in the surface layer is $J_{12}=7.4$ meV, and $J_{34}=19.8$ meV for the interface layer. This large difference reveals a strong coordination influence of the Si states on the Mn-Mn exchange interaction. Note that the number of neighboring Si atoms for a Mn atom in the interface layer is less than for the Mn atom in the surface Mn layer. The first-neighbor interlayer exchange parameters J_{24} and J_{13} are estimated as 19.6 meV and the second-neighbor interlayer exchange parameters J_{14} and J_{23} are estimated as -2.9 meV. A negative sign of the exchange parameter shows that an antiparallel spin coupling is more favorable. As a conclusion, the exchange coupling between Mn atoms depends not only on interatomic distances but also strongly on the number of neighboring Si atoms.

A. Free-standing one monolayer of MnSi

The strength of the interatomic exchange interaction is determined by the electronic structure of the system. The relation between the electronic structure and the exchange parameters is, however, very complex. The reason for this complexity can be explained as follows. The exchange parameters describe the change of the total energy of the system with the change of the magnetic configuration. The total energy is an integrated characteristic that depends on the electronic states of the system. The variation of the magnetic structure leads to a complex pattern of the changes in the electronic states. This pattern depends crucially on the energy position of the states, their spin polarization, and hybridization. The contributions to the total-energy change coming from different electronic states largely compensate each other and the final value of the total-energy variation is determined by a fine balance of interactions in the system.

Although we cannot directly predict the values of the effective exchange parameters by the analysis of the electronic DOS of the ground state, to get an insight into the role of the Si atoms in the formation of the magnetic interactions, it is instructive to compare the variation in the electron structure for a series of systems. We performed calculations for five Mn-Si films (Fig. 6). One ML of Mn atoms is the same for all films and corresponds to two Mn atoms in a (1×1) surface unit cell. The Si environment is changed systematically. From the viewpoint of the Si environment, the five systems can be characterized as follows: (i) pure Mn monolayer, (ii) a sparse Si layer on one side of the Mn ML, (iii) a dense Si layer on one side of the Mn ML, (iv) one dense and one sparse Si ML on both sides of the Mn ML, and (v) dense Si ML on both sides of the Mn ML (Fig. 6). The dense layer has two Si atoms per (1×1) surface unit cell while the unit cell of the sparse layer contains one Si atom per surface cell.

Figure 6 illustrates the influence of the Si atoms on the partial Mn $3d$ DOS. This influence is very strong and clearly reveals the important role of the Mn-Si hybridization. This hybridization leads to a broadening of the DOS in each of the spin channels that is also reflected in the decrease in the Mn moments with increasing number of the Si atoms in the near environment.

The Mn magnetic moment for an isolated Mn layer is 3.9 μ_B, which reduces to 3.4 and 2.9 μ_B for the structures (ii) and (iii) [Figs. 6(a)–6(c)].

The magnetic moment of the Mn layer sandwiched between two asymmetric dense and sparse Si layers [Fig. 6(d)] is 2.3 μ_B, which is strongly reduced to 0.8 μ_B for two symmetric dense Si layers.

The comparison of the total energies of the ferromagnetic and antiferromagnetic configurations shows that for the cases (i) and (ii), the exchange interaction between nearest Mn atoms is antiferromagnetic, whereas it becomes ferromagnetic for structures (iii)–(v). This property emphasizes again the importance of the hybridization of the Mn $3d$ states with the states of the nominally nonmagnetic Si atoms. As stated above, there is no simple way for deriving the values of the exchange interactions on the basis of the electronic structure. A possible qualitative reason for the transition from ferromagnetic exchange to antiferromagnetic exchange might be, for instance, the mechanism discussed by Kanamori and Terakura.[28]

B. Magnetic transition temperature

Now we turn to the estimation of the Curie temperature for MnSi ultrathin films. As discussed in Sec. II we apply

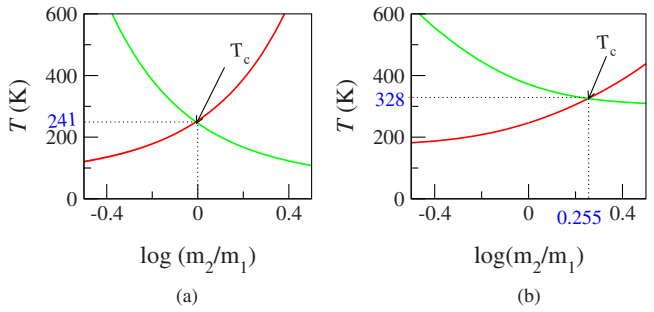

FIG. 7. (Color online) Dependence of T_c on the logarithmic scale of magnetization ratio of two sublattices for (a) a one ML and (b) a two ML MnSi films. Red and green curves belong to the sublattices in the surface and interface layers, respectively. The curves intersect at the point where $\log(m_2/m_1)$ is 0 for one ML and 0.255 for two ML films. This points correspond to the T_c of 241 and 328 K for one ML and 0.255 for two MLs, respectively. The anisotropy energy obtained by spin-orbit calculation is 0.4 meV.

two approaches: mean-field approximation (MFA) and random-phase approximation (RPA).

Within MFA and using the exchange parameters derived above, we obtain a Curie temperature of 565 and 757 K for one and two MLs, respectively. These large values of the T_c-MFA reflect strong interatomic exchange interaction. This is mainly due to the enhancement of the value of the magnetic moment in a layered structure.

To determine the Curie temperature within RPA, we plot the Curie temperature as a function of the ratio of the sublattice magnetizations for each of the two sublattices [Eq. (4)]. The intersection of the curves gives the Curie temperature of the system.

For one ML, J_{12} and J_{34} are very close to each other. The two sublattices can be considered as almost equivalent. That makes the curves $T[\log(m_2/m_1)]$ for the two sublattices almost mirror symmetric and results in the intersection of the curves close to the point $m_1=m_2$ [Fig. 7(a)].

For two ML coverage, the surfacial magnetization drops faster than the interfacial magnetization. The curves intersect at the point where the ratio of magnetizations is 1.8 [see Fig. 7(b)]. The inequivalence of the Mn layers results from the different Si environment (see Fig. 5).

In Fig. 8 we show the dependence of the Curie temperature on the anisotropy parameter for both one and two ML films. The logarithmic dependence of T_c on Δ is in agreement with the rule proposed by Bruno.[29] A calculation that includes spin-orbit interaction gives an anisotropy parameter of 0.4 meV for this system. This is comparable with the value calculated by Pajda *et al.*[30] for Fe and Co films. We obtain values of the RPA Curie temperature of 241 and 328 K for the one and two ML MnSi films, respectively. Since RPA treats properly the long-wavelength fluctuation, it gives better estimation of T_c.[14]

Due to strong ferromagnetic interlayer coupling, the Curie temperature is enhanced with increasing film thickness from one to two MLs. Additionally we calculate the Curie temperature for a free-standing two ML MnSi films without a Si substrate [this correspond to the four top atomic layer of Fig. 5(b)]. In this case the MFA approach gives a value of 211 K

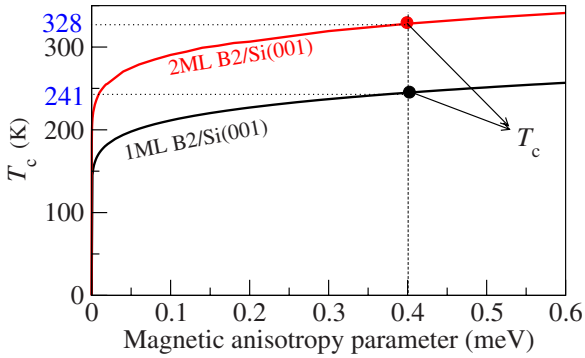

FIG. 8. (Color online) Curie temperature versus anisotropy parameter for one ML (black curve) and two ML (red curve) coverage within RPA.

while the RPA value is 135 K. Therefore, the Si substrate enhances the Curie temperature of the MnSi film significantly.

The dependence of the magnetic transition temperature on the dimensionality of the system is a nontrivial issue since the change of the dimensionality leads to changes in the system that have opposite effect on the magnetic transition temperature. The reduced coordination number of the magnetic atoms leads to a decreasing number of exchange interactions with neighboring atoms. This factor is expected to result in a decreased transition temperature. On the other hand, the decreased coordination number leads to less intense hybridization of the states of the magnetic atom with the states of the environment. Narrower energy bands are the consequence of the decreased hybridization, which can cause a strong increase in the atomic magnetic moments and interatomic exchange interactions. Whichever one of these two trends wins can be different for different systems. In our calculations we found that the strong increase in the magnetic moments and exchange interactions in the films compared to the bulk overcompensates the decreased number of the interatomic interactions and leads to an enhanced Curie temperature of the film. (See the related experimental and theoretical discussions of the enhanced Curie temperature of the Gd surface.[31,32])

V. SUMMARY

In the present work we focused our study on the calculation of the ground-state and thermodynamic magnetic properties of the bulk, free-standing, and supported films of MnSi with the B2 crystal structure. We show that decreasing the coordination number of the Mn atoms in the MnSi film leads to an increase in the magnetic moments, the exchange interactions, and the magnetic transition temperature compared to the bulk system. Also, the Si substrate increases the Curie temperature of MnSi film. To get a deeper insight into the role of Si, we perform calculation of a Mn monolayer with different Si environments, and demonstrate that increasing Si coordination of Mn atoms stabilizes ferromagnetism. We study the dependence of the Curie temperature of the films on the magnetic anisotropy energy that has a weak logarith-

mic character. For the calculated magnetic anisotropy energy of 0.4 meV per Mn atom, the Curie temperature assumes the value of 241 and 328 K for one and two ML MnSi films, respectively.

ACKNOWLEDGMENT

This work was supported by the Deutsche Forschungsgemeinschaft through Research Center SFB 290.

[1] H. Wu, M. Hortamani, P. Kratzer, and M. Scheffler, Phys. Rev. Lett. **92**, 237202 (2004).
[2] M. Hortamani, H. Wu, P. Kratzer, and M. Scheffler, Phys. Rev. B **74**, 205305 (2006).
[3] M. Hortamani, Ph.D. thesis, Freie Universität, Berlin, 2006.
[4] H. Wu, P. Kratzer, and M. Scheffler, Phys. Rev. B **72**, 144425 (2005).
[5] M. Hortamani, P. Kratzer, and M. Scheffler, Phys. Rev. B **76**, 235426 (2007).
[6] A. I. Liechtenstein, M. I. Katsnelson, V. P. Antropov, and V. A. Gubanov, J. Magn. Magn. Mater. **67**, 65 (1987).
[7] J. MacLaren, T. Schulthess, H. Butler, R. Sutton, and M. McHenry, J. Appl. Phys. **85**, 4833 (1999).
[8] R. Zhang and R. F. Willis, Phys. Rev. Lett. **86**, 2665 (2001).
[9] The concept of using model Hamiltonian in which parameters are determined by DFT calculation is a standard approach which is used before; For example, in the lattice-gas Hamiltonian approach, see C. Stampfl, H. J. Kreuzer, S. H. Payne, H. Pfnur, and M. Scheffler, Phys. Rev. Lett. **83**, 2993 (1999).
[10] Y. G. Sinai, *Theory of Phase Transitions: Rigorous Results* (Pergamon, Oxford, 1982).
[11] N. D. Mermin and H. Wagner, Phys. Rev. Lett. **17**, 1133 (1966).
[12] P. W. Anderson, *Solid State Physics*, edited by F. Seitz and D. Turnbull (Academic Press, New York, 1963), Vol 14, pp. 99–214.
[13] E. Sasioglu, L. M. Sandratskii, and P. Bruno, Phys. Rev. B **70**, 024427 (2004); **71**, 214412 (2005); E. Sasioglu, L. M. Sandratskii, P. Bruno, and I. Galanakis, *ibid.* **72**, 184415 (2005).
[14] J. Rusz, I. Turek, and M. Divis, Phys. Rev. B **71**, 174408 (2005).
[15] E. Sjöstedt, L. Nordström, and D. J. Singh, Solid State Commun. **114**, 15 (2000).
[16] P. Blaha, K. Schwarz, G. K. H. Madsen, D. Kvasnicka, and J. Luitz, *WIEN2k, An Augmented Plane Wave Plus Local Orbitals Program for Calculating Crystal Properties* (Karlheinz Schwarz, Technical Universitat Wien, Austria, 2001).
[17] Y. Ishikawa, K. Tajima, P. Bloch, and M. Roth, Solid State Commun. **19**, 525 (1976).
[18] M. R. Krause, A. J. Stollenwerk, J. Reed, V. P. LaBella, M. Hortamani, P. Kratzer, and M. Scheffler, Phys. Rev. B **75**, 205326 (2007).
[19] P. Kratzer, J. Hashemifar, H. Wu, M. Hortamani, and M. Scheffler, J. Appl. Phys. **101**, 081725 (2007).
[20] T. Moriya, Solid State Commun. **26**, 438 (1978).
[21] H. von Känel, C. Schwarz, S. Goncalves-Conto, E. Müller, L. Miglio, F. Tavazza, and G. Malegori, Phys. Rev. Lett. **74**, 1163 (1995).
[22] T. Jeong and W. E. Pickett, Phys. Rev. B **70**, 075114 (2004).
[23] C. Thessieu, C. Pfleiderer, A. N. Stepanov, and J. Flouquet, J. Phys.: Condens. Matter **9**, 6677 (1997).
[24] E. Stoner, Proc. R. Soc. London, Ser. A **154**, 656 (1936).
[25] J. F. Janak, Phys. Rev. B **16**, 255 (1977).
[26] P. James, O. Eriksson, B. Johansson, and I. A. Abrikosov, Phys. Rev. B **59**, 419 (1999).
[27] E. Sasioglu, I. Galanakis, L. M. Sandratskii, and P. Bruno, J. Phys.: Condens. Matter **17**, 3915 (2005).
[28] J. Kanamori and K. Terakura, J. Phys. Soc. Jpn. **70**, 1433 (2001).
[29] P. Bruno, *Magnetization and Curie temperature of ferromagnetic ultrathin films: The influence of magnetic anisotropy and dipolar interactions*, MRS Symposia Proceedings No. 321 (Materials Research Society, Pittsburgh, 1992), p. 299.
[30] M. Pajda, J. Kudrnovsky, I. Turek, V. Drchal, and P. Bruno, Phys. Rev. Lett. **85**, 5424 (2000).
[31] A. B. Shick, W. E. Pickett, and C. S. Fadley, Phys. Rev. B **61**, R9213 (2000).
[32] M. Farle and K. Baberschke, in *Magnetism and Electronic Correlations in Local-Moment System*, edited by M. Donath, P. A. Dowben, and W. Nolting (World Scientific, Singapore, 1998), p. 35.